Advanced Structural Mechanics 1 (2023) 229-241

Advanced Structural Mechanics

Journal homepage: http://asm.sku.ac.ir

Effect of statistical parameters of roughness distribution on the analysis of contact problem

Arman Mozaffary[a], Ali Moazemi Goudarzi[a], Fattaneh Morshedsolouk[a]*

[a]*Babol Noshirvani University of Technology, Iran, Babol, Shariati Avenue, 4714871167*

Article received:2023/11/6, Article revised: 2023/11/26, Article accepted: 2023/12/1

ABSTRACT

In this research, studies on the behavior of contact mechanics among other surfaces have been presented according to the statistical functions. Also, with the knowledge of the statistical parameters of roughness, the certain area roughness of the studied surfaces has been predicted by using a Gaussian statistical function. The obtained data is the base for defining the geometry of the surfaces that contact together. In fact, by modeling the surface geometry, the mechanical behavior of the two contacted surfaces has been calculated in two different conditions as follows: loading conditions of 500 and 5000 micro-Newton by finite element method. The elastic and plastic behaviors of the involved surfaces are investigated under two loading conditions and considered in detail. At some point, examples such as the quality of contact surfaces in the macroscopic scope, contact area, the height of vertices, and weight function are discussed. The result shows that the roughness of the surface is undesirable, but it is a stress-intensifying factor. Regarding the statistical characteristics of the roots-mean-square, it can be concluded that the shrinkage of the roots-mean-square of the surface leads to a decline in the height of the vertices in the surface, which in turn results in a decrease in contact stress.
Keywords: Rough surface, Contact mechanics, Asperity, Mathematical models;

1. Introduction

In a tribological manner, it is important to determine the contact properties of the involved rough surfaces accurately. In practice, the real contact surface resulted from contact is smaller than that of the nominal surface. The external loads act on two surfaces, which are tolerated by the surfaces' peaks, causing higher compression stresses comparing to the ideal state.

Greenwood and Williamson (GW) assumed a contact model for contacting two rough surfaces using a Gaussian distribution. In the GW model, it was assumed that the curvature of all roughness is the same and only their heights vary [1]. After the GW model, the classical models with different assumptions on surface roughness were applied.

* Corresponding author at: Babol Noshirvani University of Technology, Babol, Iran.
E-mail address: goudarzi@nit.ac.ir
DOI: 10.22034/asm.2023.14570.1017: https://asm.sku.ac.ir/article_11532.html

They were based on the statistical models and the assumptions on the shape of roughness with a certain width and height, which were considered intending to simplify the contact issue [2-5].

Over recent years, researchers have analyzed real rough surface behavior using the finite element method from the viewpoint of the experimental model [6]. Infinite element simulation of contact can consider the real material and surface properties, and the complex geometry of the structure and various boundary conditions. It is one of the unique features of the analysis based on the finite element method. Poon and Sayles [7] studied the effect of surface roughness on the quantity of real surface contact for the elastic-plastic contact of a polished ball with anisotropic surface roughness. Lee and Cheng [8] used a numerical model to simulate the contact between two rough surfaces whose roughness was considered only in the longitudinal direction. At that time, a computer simulation was very time-consuming. Kucharski, et al. [9] analyzed the finite element of contact between an elastic-plastic sphere and a rigid surface; and compared the results with the elastic model of GW and the elastic-plastic model proposed by Chang, Etsion and Boggy (CEB). It is concluded that the results of the simulation of finite elements are close to experimental results.

Sellgren, et al. [10] conducted contact analysis for rough surfaces with the real engineering surface properties using the finite element method. They found the effect of distribution of roughness's height to be significant on the contacting surface hardness, but insignificant on the curvature's radius of roughness. Pei, et al. [11] produced a rough surface using a continuous random midpoint algorithm whose random midpoints were based on the fractal statistical distribution. They modeled a non-frictional and non-sticky contact between a rigid surface and an elastoplastic rough solid by using the finite element method. Their results showed that the real contact surface changes linearly by increasing the load. Nadimi, et al. [12] showed that in the absence of interlocking, rough particle surfaces exhibit a lower frictional resistance in comparison with equivalent smooth surfaces. Krithivasan and Jackson [13] analyzed the contact between three-dimensional sinusoidal roughness and rigid surface in an elastoplastic zone by ANSYS commercial software. They equalized the real contact surface formulation and contact pressure for sine roughness in the elastic-plastic regime based on finite element analysis. As an alternative modeling of contact loaded normally and tangentially, the non-statistical multi-scale model was also applied. As a first step, an elastic–plastic sinusoidal waviness contact under normal and tangential loading was considered by Wang et al. [14]. Zhao et al. [15] applied the Persson contact mechanics theory to metallic seals where plastic deformations are important unless the surfaces are extremely smooth. Experimental studies of plastic deformation of rough metallic and polymeric surfaces are presented in Refs. [16]. Several studies on surface roughness and plastic flow have been reported using microscopic (atomistic) models [17], or models inspired by atomic scale phenomena that control the nucleation and glide of the dislocations [18–21]. Persson and Tiwari studied the nominal (ensemble averaged) contact pressure acting on a cylinder squeezed in contact with an elastic half space with random surface roughness using Hertz and Gaussian methods to analyze the dry contact [22].

The creation of rough surfaces is generally based on two statistical and definitive views. The statistical view is based on statistical approximation and randomized analysis of contact surfaces' roughness model [23]. Various statistical functions have been proposed for the distribution of roughness height, such as exponential distribution, Gaussian distribution, power series, Fourier series, and fractal series. Several studies have evaluated the effect of the type of distribution function on the contact mechanics' model [24]. In some studies, the analysis of contact properties of rough surfaces was carried out by Gaussian distribution using various methods. For example, Patir [25]. used a linear transformation to create a roughness point matrix. For the first time, the autocorrelation function was proposed to produce a rough Gaussian surface containing M, N points. First, the simulation of Gaussian rough surfaces was performed in a form of rough points sequential two-dimensional spectrum and then, in a rough surface form. Newland presented a model to generate rough surface using the fast Fourier transform function and circular autocorrelation function [26]. The fast Fourier transform (FFT) is defined for a series of finite points to have discrete direct and inverse Fourier transformations. One of the important features of FFT is that a large amount of data from roughness points can be simultaneously handled. Wu presented a model using the Newland model, the fast Fourier transform method and the autocorrelation function model [27]. Reizer [28] simulated the measured rough surface based on Gaussian and non-Gaussian rough surfaces by using Wu and Newland numerical model through FFT. They then compared the statistical data of the measured surface and modeled the rough surface. Yastrebov, et al. [29] introduced a corrective function to compensate for errors in contact area computations coming from mesh discretization. The correction is based on geometrical arguments and requires only one additional quantity to be computed: the length of contact/non-

contact interfaces. There are simplifications in the analysis of mutual interactions of asperities. To have a mesh sufficiently fine for fair analysis of deformation on the level of individual asperity, one requires a very long time of calculations that may be not acceptable. This effect manifests as a low accuracy of the deterministic model at the beginning of contact when the number of finite elements touching the counter surface is inadequate [30]. Jacobs et al. [31] presented three important drawbacks that impede the application of power spectral density to the functional characterization of surface topography and proposed strategies to mitigate them.

Reviewing the literature, it can be deduced that the method for modeling the surface is not fully investigated. This research is focused on modeling the surface using statistical parameters and Spline tool, as well as investigation of the contact parameters for two three-dimensional objects in contact. The rough surface is created statistically by applying the autocorrelation function as well as by FFT to randomly create rough points. A solid surface is then generated using the mathematical method and available commercial CAD software model. At the next step, solving the finite element for the contact of rough surfaces with various roughness sizes, and comparing them with each other under different compressive forces imposing the objects involved have been accomplished, and a nomenclature is put forth if necessary, in a box with the same font size as the rest of the paper. The paragraphs continue from here and are only separated by headings, subheadings, images, and formulae. The section headings are arranged by numbers, bold and 10 pt. Here follows further instructions for authors.

2. Generation of random rough surfaces

Most surfaces are expressed in the form of a matrix of the points' coordinates obtained from the measurement.

$$z = f(x, y) \tag{1}$$

where z is the surface profile and x, y are the surface coordinates. The z parameter is the height of roughness points based on a function of coordinates x and y. The autocorrelation function is expressed in the discrete form to make a continuousness among the roughness points as below:

$$R(x, y) = {R_q}^2 \, exp\left[-2.3\sqrt{\frac{x^2}{\beta_x} + \frac{y^2}{\beta_y}}\right] \tag{2}$$

where β_x, β_y and R_q are distances in two orthogonal directions and the average square of the roots, respectively.

The roughness output sequence for $n \times m$ points with different heights can be expressed from the combination of the autocorrelation function and the finite impulse response filter method presented by Hu and Tonder [32]:

$$\begin{gathered} Z_{p.q} = \sum_{r=0}^{m-1} \sum_{s=0}^{n-1} h_{r.s} \, \eta_{p+r.q+s} \\ p = 0, 1, 2, \ldots, m-1 \\ q = 0, 1, 2, \ldots, n-1 \end{gathered} \tag{3}$$

where $\eta_{r.s}$ is the collection of random points that are created by the Gaussian distribution and $h_{r.s}$ is the restricted finite impulse response filter for the three-dimensional state, and its fast Fourier transform function is called the transfer function, which is based on the autocorrelation function.

$$\begin{gathered} H_{k.l} = \sum_{r=0}^{m-1} \sum_{s=0}^{n-1} h_{r.s} \, exp\left(2i\pi\left[\frac{kr}{m} + \frac{ls}{n}\right]\right) \\ k = 0, 1, 2, \ldots, m-1 \\ l = 0, 1, 2, \ldots, n-1 \end{gathered} \tag{4}$$

The simulation of rough surfaces uses the Gaussian distribution in the generation of random spatial points based on its FFT function as follows:

$$Z_{k.l} = H_{k.l}A_{k.l} \tag{5}$$

where $A_{k.l}$ is the FFT of random points as below:

$$A_{k.l} = \sum_{r=0}^{m-1}\sum_{s=0}^{n-1}\eta_{r.s}ex\,p\left(2i\pi\left[\frac{kr}{m}+\frac{ls}{n}\right]\right) \tag{6}$$

The Gaussian simulation of points is formulated using the mentioned method and the specified autocorrelation function through a mathematical commercially available software to produce surfaces' roughness.

2.1. Mathematical approximation using Spline method

The well-known Spline method treats so that all provided points are to be passed. In this method, the division of the intervals among the points and passing the curve resulted from the interpolation are used. The roughness approximation function must pass through all the points of roughness and be continuous and differentiable along the path through the roughness. In other words, in the interval $[x_0, x_1]$, one should pass a polynomial function whose amount in x_0 and x_1 equals to that of the measured roughness. By proceeding this process on the entire interval, the interpolation polynomial function is specified segment by segment. The cubic spline polynomials satisfy the continuity condition of the curve, as well as boundary conditions. Hence, it is the best one to model the curve [33]. A cubic polynomial, for a given y, is as follows:

$$S(x) = ax^3 + bx^2 + cx + d \tag{7}$$

If there are n points of a set of roughness to describe the geometry of 2D profile, then a cubic spline interpolation function associated with the points is a function S that satisfies the following conditions:

1. S is a third-order polynomial. For simplicity, the S function over the interval $[x_j,\ x_{j+1}]$, in which $j = 0,1\ , \dots , n-1$, is denoted by S_j.
2. $S(x_j) = F(x_j)$, for $j = 0.1 \dots n$.
3. $S_{j+1}(x_{j+1}) = S_j(x_{j+1})$, for $j = 0.1 \dots n-2$.
4. $S'_{j+1}(x_{j+1}) = S'_j(x_{j+1})$, for $j = 0.1 \dots n-2$.
5. $S''_{j+1}(x_{j+1}) = S''_j(x_{j+1})$, for $j = 0.1 \dots n-2$.

There are two boundary conditions at the left and right of the roughness domain:

$$S'(x_n) = f'(x_n)\text{ ، }S'(x_0) = f'(x_0) \tag{8}$$

For the cubic spline polynomial, the constants a, b, c, and d are the unknowns of every single roughness.

For the cubic spline polynomial, the constants a, b, c, and d are the unknowns of every single roughness.

The conditions Eqs. (2-5) make $n+1, n-1,\ n-1$ and $n-1$ equations, respectively. The total is $4n-2$ equations to solve $4n$ unknowns. By adding the boundary conditions, namely Eq. (8), to the set of equations, one can find a set of equations included $4n$ equations and $4n$ unknown coefficients of the cubic spline function to be solved.

According to the cubic spline curves passing from every two adjacent points on horizontal and vertical directions (points to coordinates (x_j,y_j,z_j), $(x_j,y_{j-1},z_{j,j-1})$, $(x_{j-1},y_j,z_{j-1,j})$, $(x_{j-1},y_{j-1},z_{j-1,j-1})$) a bicubic-spline patch procedure can be defined in which the cubic spline curves refer to its boundaries and the points mentioned in its corners. Based on the defined patch, roughness height coordinates can be calculated at each point located between the points of the corner.

To examine the effect of the distances of the autocorrelation function, a rough surface of $30\ \mu m \times 30\ \mu m$ in the area is considered so that it is characterized by the roots mean square coefficient of 0.4 for autocorrelation intervals of 1, 5 and 10 μm and by 2 μm dividing intervals along x and y.

The surface approximated by the cubic spline method is shown in Fig. 1 for the different ratios (β/Δ). It should be noted that β and Δ are the intervals of the autocorrelation function and the random point intervals, respectively. The intervals of the autocorrelation function have changed the surface properties, also, the roughness pattern of the surface is declined by the increase in the intervals of the autocorrelation function.

To investigate the effect of root mean square of the surface roughness, three different Gaussian' isotropic rough surfaces have been generated using the mentioned modeling method (Fig. 2). The surfaces of 30×30 μm^2 in the area are established with different roots mean square coefficients $R_q$of 0.004 m, 0.04 m and 0.4 m and autocorrelation of 1 m, as well as sampling with 2 m intervals in both directions x and y.

Due to the decrease in the roots mean square, the height of roughness decreases, and the mean of roughness height approaches to zero. In Fig. 2, the surface of the lowest and highest roughness are related to $R_q = 0.004$ and R_q=0.4, respectively.

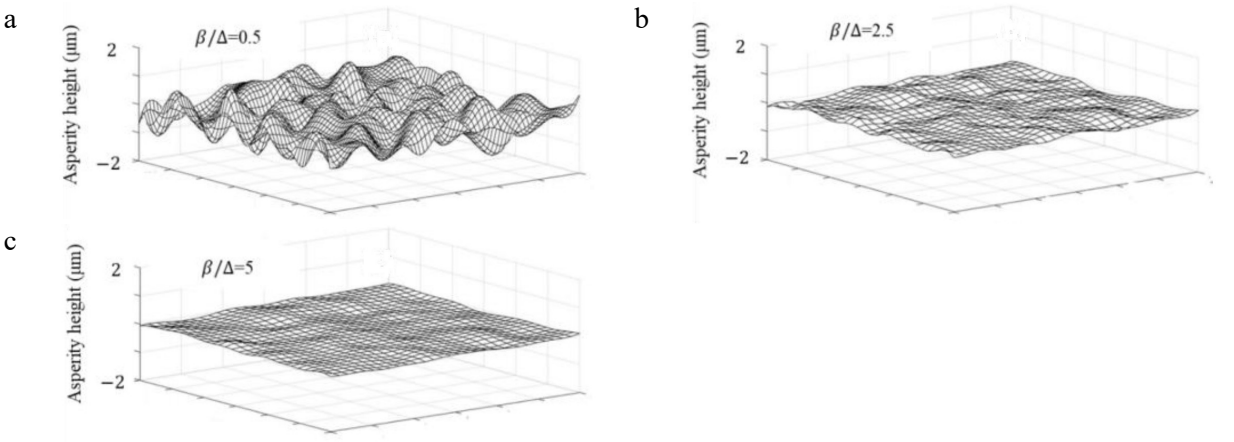

Fig. 1. Generation of Gaussian rough surfaces which is approximated by spline for (a) (β/Δ).=0.5; (b) (β/Δ).=0.25; (c) (β/Δ).=0.5

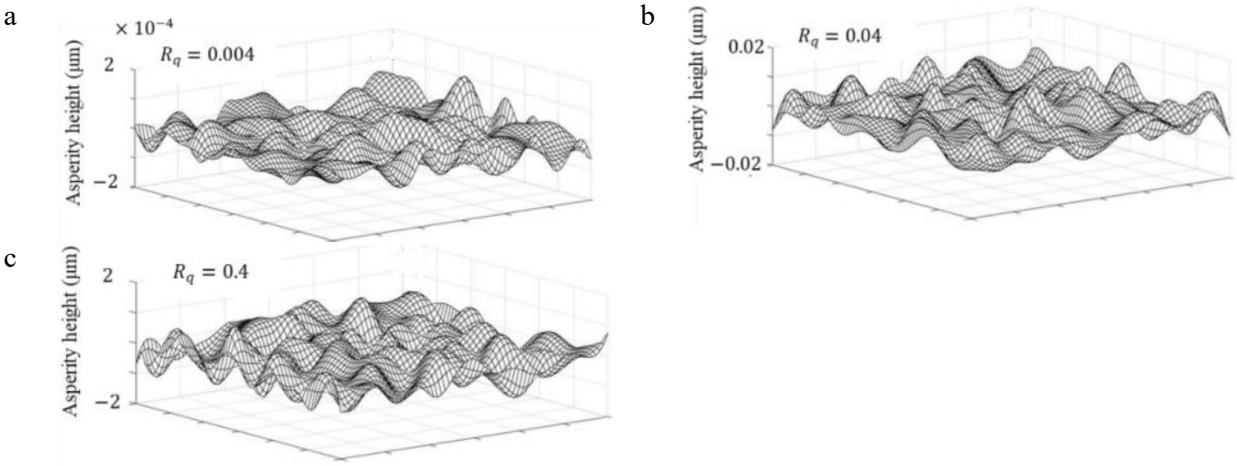

Fig. 2. Generation of Gaussian rough surfaces which is approximated by spline method with varied root mean square (a) $R_q = 0.004$; (b) $R_q = 0.04$; (c) R_q=0.4.

2.2. Surface modification

SolidWorks software is used to apply the data derived from generated rough surface data to produce a realistic surface. The surface data matrix is imported into the graphical environment as a cloud of points.

The algorithm of procedure for producing the geometry of the rough solid is briefly expressed as follows:

- Align the characteristics of the cloud of the points with the reference point and the surfaces.
- Clear the points that are out of the average distribution. This removes the noise-making points from the results.
- Smooth the boundary points and surface of the edges if necessary.
- Fill the holes if necessary.

It is worth mentioning that by applying the algorithm of removing the noise from points cloud, existing in numerical analysis software, one can also reduce the number of points imported without any change in geometry of the surface. The advantage of this algorithm is that a smaller file (in size) is finally generated.

3. Modeling and analysis of rough surfaces

The generated rough surface is a facet of cube geometry that interact with a smooth surface by imposing a vertical external force. Intervals of roughness distribution in both directions x and y are equal to 2 μm. The cubes are modeled in finite element analysis software as a flexible solid. They are made of aluminum alloy AA6060 whose mechanical properties are presented in Table 1. It is worth mentioning that the smooth surface is considered rigid. The external load is imposed on the rigid body (see Table 2).

To improve the present analysis, the hexagonal brick elements with reduced formulation (C3D8R) has been used to solve the problem. The 3D meshing of flexible solid is shown in Fig. 3. As can be seen, the upper side of the cube is considered as a rough surface. Regarding the complexity of the contact analysis, the explicit solver is used. With attention to the contact models and type of analysis, general contact definition is the most appropriate to determine the contact between the involved surfaces.

4. Results and discussion

The contact analysis should be fundamentally solved incrementally. The results of the contact solution are step-by-step derived in any load step. The normal loading resulting from the two involved objects is calculated by the sum of contact force values-oriented in z-direction for each node. The real contact area is calculated by summing the total area of the involved elements due to external loading.

It is noted that the rough surface in this study is considered a small part of a much larger surface. It follows that the vertically component of the applied force on the body is a small contribution of the total force. Accordingly, the modeled rough surface has been analyzed and it is subject to a load of 500 micro-Newton.

To compare and examine the effects of roughness between the involved surfaces, the results of the contact analyses are presented in a non-dimensional manner and are also expressed in terms of the geometric properties of surfaces. Henceforward, in all presented curves, the penetration values and contact normal force values are made dimensionless by the highest peaks of each surface (d/z_{max}) and external normal force on the surfaces (F_n/F_t), respectively. Also, the real contact area is made dimensionless by the nominal contact area (A_{real}/A_{nom}). Finally, the maximum stresses are made dimensionless by yield stresses of the material (σ_{max}/σ_y).

Table 1. Material parameters for aluminium alloy AA6060 [34].

Density $[kg/m^3]$	Young's modulus $[GPa]$	Poisson's ratio	Yield stress $[MPa]$
2700	26.1	0.32	79.4

Table 2. Case studies for the external loading

Investigated cases	External force [μN]
Case 1	500
Case 2	5000

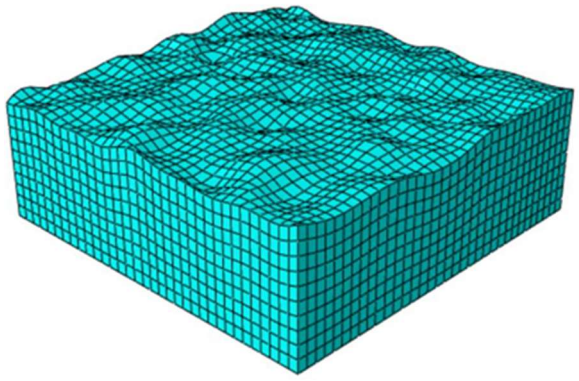

Fig. 3. The 3D meshing of flexible solid with ACL=1 and R_q=0.4.

4.1. Effect of the weight Function on contact parameters

An increase in the real contact area to the nominal one versus the dimensionless contact load has been defined as the normal force to the external force which is shown in Fig. 4. By increasing the contact load between the two surfaces from the beginning of the contact until the normal force is fully transferred, the real contact area development rate increases in all three rough case studies.

The body with β/Δ=5 has the largest involved area. The reason for this fact is that the rough surface of β/Δ=5 is modeled more widely and more shortly. It means that the contact forces between the two involved bodies are applied to their asperities, not to the nominal areas. Therefore, ignoring the quality of the machined surfaces results in a significant error in the contact issue. As can be seen, by increasing the contact forces, the number of the involved asperities is increased, and the real contact area could be closer to the nominal contact area. The maximum real contact area for the object with the most weight function is about 0.44% of the nominal contact area.

Figure 5 shows the distribution of the contact forces due to the interaction of the rough surface with the rigid one. Evaluating the effect of the intervals of autocorrelation functions on surface modeling approaches reveals that the slope of the contact force curve versus vertical displacement of the rigid surface is sharper by decreasing in β/Δ. It is also seen that the more the β/Δ decreases, the more the nonlinear behavior in the curve.

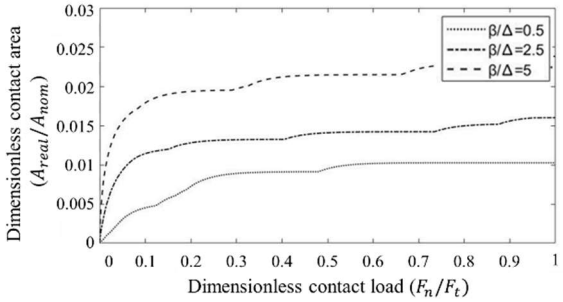

Fig. 4. Dimensionless real contact area versus dimensionless contact load.

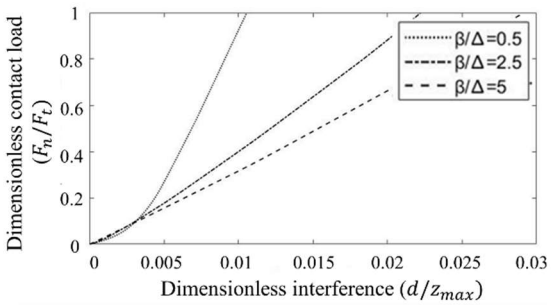

Fig. 5. Dimensionless contact load versus dimensionless interference.

The important key is to increase the interference of the surfaces through an increase in the contact load. The smaller the distance of autocorrelation function, the larger the penetration of the surfaces and vice versa. The amount of surface interference is 0.00087 μm when autocorrelation function is β/Δ=5, whereas it is 0.0021 μm when the distance of autocorrelation function is decreased β/Δ=0.5. The same value associated with the body of β/Δ=2.5 is 0.00072 μm. As shown in Fig. 5, the rate of the interference reduces when β/Δ increases. As shown in Fig. 5, the increase in the contact force causes the difference between the penetration value in the surface of β/Δ=0.5, and the surfaces of smaller roughness have an upward trend. The reason for this fact is that the roughness and contact area are larger and smaller, respectively. In other words, the total force is applied to the small area and so, the high contact pressure exists in the contact area.

The dimensionless maximum contact stress versus the dimensionless contact load between the two involved surfaces is shown in Fig. 6. It can be seen from Fig. 5 and 6 that the surface roughness of the weight function β/Δ=0.5 has the most deformation and, consequently, the greatest contact stress compared with the other surfaces. It is followed by the fact that the contact force is applied to a limited amount of roughness, and the small area of the total nominal area of the surface is thus affected by the contact load. The smallness of the real contact area results in the high-pressure force on the rough surface of the weight function β/Δ=0.5 and, in turn, causes the deformation of the body to occur beyond the yielding point of the material. By more precise observation in Fig. 6, one can find out that the increase in the number and the magnitude of roughness leads to an increase in the nonlinearity of the problem.

In theoretical analyses, to study the elastic-plastic analysis of contacts, the researchers commonly use the average pressure as a criterion of the yielding. In the present study, unlike the theoretical analyses, the Von-Mises' equivalent stress is used to move the material from the elastic zone to the plastic regime. For the rough surface to pass through the elastic zone, the applied external force between the two bodies is increased up to 5000 μN, causing the interference between the rough and rigid surfaces to grow.

Figure 7 shows the real contact area versus non-dimensional interference. In the present study, the smallest contact area belongs to the model of β/Δ=0.5 and the largest one is associated with the model of β/Δ=5. At the end of loading process, for three contact areas according to the increase in the weight functions, the real contact area increases by 1.66%, 2.53%, and 3.36% compared to the nominal area of the Hertz roughness-free theory, respectively.

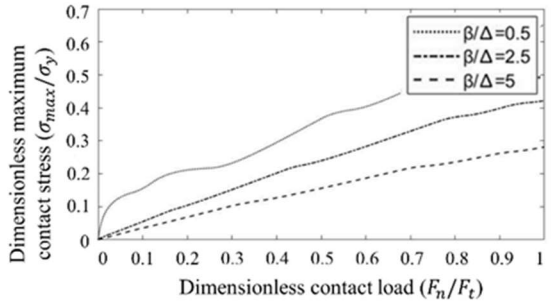

Fig. 6. Dimensionless maximum contact stress versus dimensionless contact load.

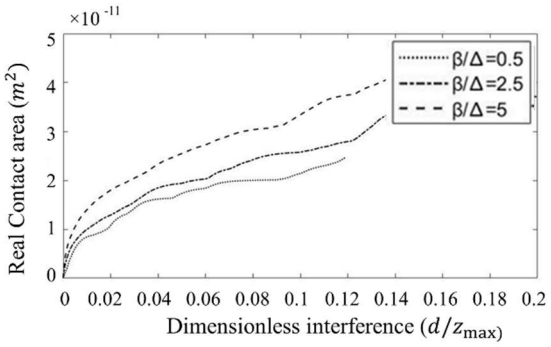

Fig. 7. Variation of the real area of contact concerning dimensionless interference.

As shown in Fig. 8, an increase in the height and number of surface roughness results in contact analysis to be more nonlinear. As presented in this figure, the difference between the maximum contact stresses of three case-study surfaces increases with enlarging the external force. Regarding the shape of roughness, all models of β/Δ=0.5, β/Δ=2.5 and β/Δ=5 move beyond the yield stress, and they have thus plastic deformation. As shown in Fig. 8, in three case-study surfaces, the increase in contact load leads to the growth of contact-induced stresses in rough surfaces. Also, with a reduction in the weight function, the asperities of the surface come to a yielding point at smaller contact loadThe model of β/Δ=0.5 reached to the plastic regime at a smaller contact load in comparison with two other models. The necessary contact forces to pass through the yielding point of the material, in terms of an increase in weight functions of three specimens, are 313.61 μN, 1095.1 μN, and 1681.2 μN, respectively. The surface of the weight function β/Δ=5 has less stress than that of the weight function β/Δ=0.5 due to the less complexity in contact geometry. Therefore, the model of β/Δ=5 touched the yielding stress with the larger value of the contact load relative to the other models. The greatest number of asperities in the model with β/Δ=5 fall in the elastic zone and small deformation.

4.2. Effect of root mean square on contact parameters

Figure 9 shows changes in the real contact area versus the non-dimensional contact force. As can be observed, increasing the magnitude of the force causes the real contact area to grow for all specimens. As shown and expected, the real contact area of the more-asperity-height surface is less than that of a smoother surface in the same contact load. As shown in Fig. 9, the real contact area approaches the Hertz roughness-free contact area by decreasing the asperity size. In other words, the real contact area to the nominal area ratio changes concerning the root mean square such that by decreasing the root mean squares, it is obtained to be about 0.0044, 0.085 and 0.9973 at the end of the loading. It is worth mentioning that the slope of real contact area versus contact load curve increases by decreasing the height of asperities. It appears the reason is that the smaller asperities have not enough stiffness to withstand the contact forces.

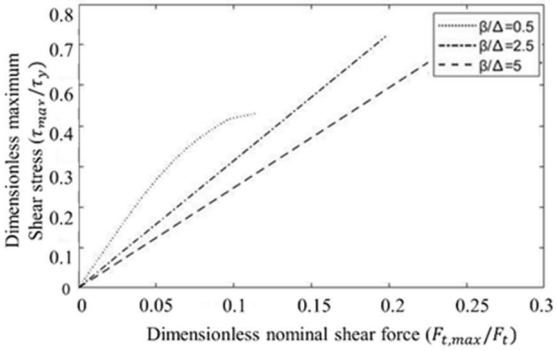

Fig. 8. Dimensionless maximum contact stress versus dimensionless contact load.

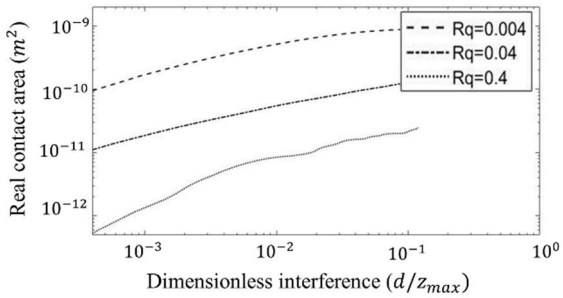

Fig. 9. Dimensionless real contact area versus dimensionless contact load.

Figure 10 presents the variations in the contact force in terms of the interference for three root mean squares. As shown in Fig. 9 and 10, the contact forces on the asperities are more smoothly distributed due to the increase in the contact area and the asperities undergo fewer variations. As can be seen in Fig. 10, the slope of changes in interference is increased as the contact force grows. It means that the smaller the asperities of the surface, the more deformed they are. In other words, the ratio of change in height of the deformed asperity to its initial height is increased when its initial height is decreased smaller. The presence of roughness is an effective factor in the transfer of the load from a body to another one. It is also noticeable that the roughness has an undesirable effect on surface design.

Figure 11 shows the maximum contact stress versus the contact load. From this Figure onward, because of more smallness of the derived parameters compared to each other, the division of the intervals of the graphs is logarithmically accomplished due to the capability of more clear descriptions. As seen in Fig. 11, the rough surface of $R_q = 0.4$ has the most value of contact stress compared to the other two models. As is evident in Fig. 11, by decreasing the roots mean square, to pass through the yielding point of the material and the beginning of the plastic deformation, the required contact force becomes larger because of the involvement of too many vertices. It can be said that the more smallness of the magnitude of asperities leads to the reduction of stress concentration. From now on, the three solids are subject to the larger force; namely 5000 μN.

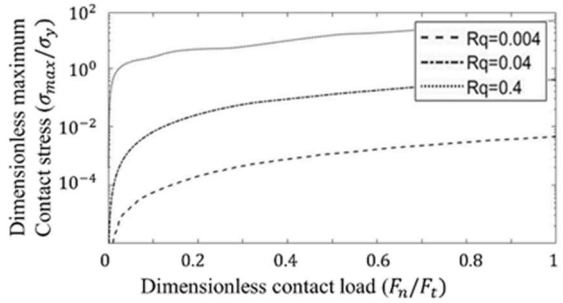

Fig. 10. Variation of dimensionless contact load in terms of dimensionless interference.

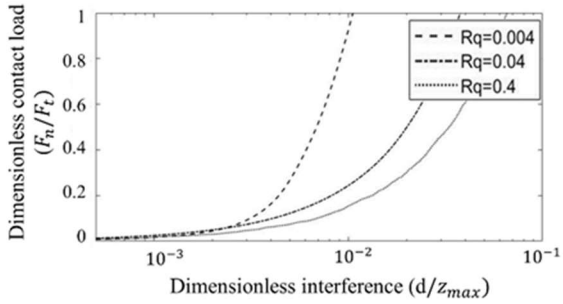

Fig. 11. Dimensionless maximum contact stress versus dimensionless contact load.

Figure 12 illustrates the real contact area of the statistical rough surfaces versus the non-dimensional interference. By surveying the diagrams of the three surfaces, it can be found that by increasing the degree of interference and the involvement of more asperities, the contact area also increases. However, this parameter in the surface with R_q=0.004 is equal to the nominal area due to asperities being very small and having a low effect on intensifying the distribution of force in a particular zone of the surface. It can result in the fact that the smaller the magnitude of the asperities, the better the force can be transferred between the two involved surfaces.

Figure 13 displays the maximum contact stress versus interference for the three root mean squares. As aforementioned, the ratio of the maximum contact stress to the yielding stress is used as the non-dimensional maximum contact stress. The variation of the non-dimensional maximum contact stress versus the non-dimensional interference in the model of R_q=0.4 increases more sharply in the elastic regime than in the plastic one. In other words, when the contact stress of the asperities is smaller than the yielding stress, the asperities do not undergo the plastic deformation. By increasing the interference, and hence moving beyond the yielding stress, the stress of the model R_q=0.4 increases. However, changes in stress are smoother. The reason for this issue is the new asperities of the involved surface and toleration of a significant part of the external loading.

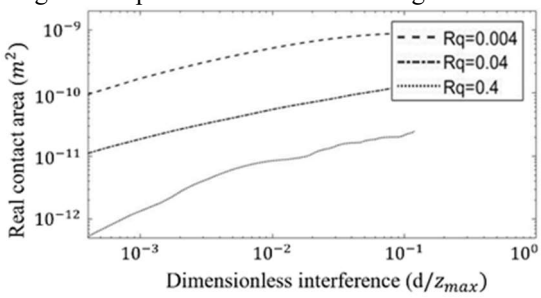

Fig. 12. Variation of the real area of contact in terms of dimensionless interference.

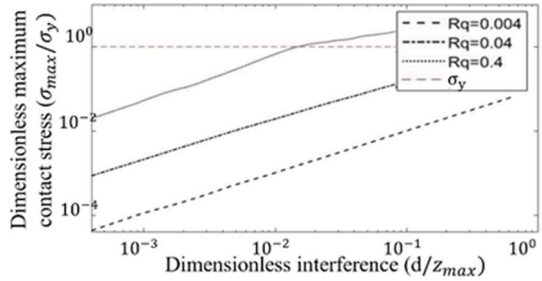

Fig. 13. Dimensionless maximum contact stress versus dimensionless interference.

The critical penetration value of the model R_q=0.4 is equal to R_q=0.0014 μm. Two other specimens undergo the plastic deformation under larger forces as compared to the model R_q=0.4.

5. Conclusion

This research evaluates the effect of roughness on contact stresses and real contact area in the three-dimensional models for a cubic solid. The surface roughness of the solid is constructed using statistical functions to randomly generate spatial points and to apply the FFT method. Using the geometry defined by statistical approximation and the numerical analysis, one can exactly identify the points of the geometry of the model to analyze. Modeling the points is performed by the cubic spline approximation and realistic implementation in SolidWorks. Numerical analysis and

surface meshing are studied in ABAQUS commercial software. The results of the analysis of contact parameters are investigated by surveying deformation and height of asperities. The results are classified as follows:

- To study the contact force distribution, the quality of contact surfaces in the macroscopic scope is of great importance in the transfer of force between the contact surfaces. Therefore, the effects of roughness is required to be taken into account in the selection of the process of manufacturing engineering surfaces, as well as their design. It is an important key that consideration of only a correction factor to calculate the contact parameters did not lead to reliable results.
- The real contact area plays a crucial role in calculating the stress-induced on the surface. In other words, it can be said that the roughness is an effective and undesirable factor in calculating the values of contact parameters. The imposed external force between the two surfaces is tolerated by the high vertices of the surface at the beginning of the conflict. This is due to the remarkable differences between the true stresses and real contact area with the nominal stresses and nominal contact area, respectively.
- The smaller the height of asperities and the greater the width of them, the more the results tend to those of Hertz's model. The reason is that the real contact area is closer to the nominal contact area by the decrease in the height of vertices and the number of the asperities. In general, the normal contact stress of the roughness-free surface experiences the smaller values than the stress of the rough surface due to the uniform distribution of the force on the surface and the less plasticity flow. The growth of normal force causes the more plasticity flow at the interface of the two bodies; however, the contact stress is larger with the lower rate. One of the reasons for this event is that the changes in the contact area are not severe in the plastic regime and are fixed at the end.
- As the weight function increases, the contact area of the body bearing the force increases.
- By decreasing in weight function, the curve of the maximum contact stress versus the normal force has a sharper slope.
- Increasing the weight function causes the roughness to be more widespread and to proceed towards the ideal model.

The roughness of the surface is an undesirable but stress-intensifying factor. Regarding the statistical characteristics of the roots mean square, it can be concluded that the shrinkage of the roots means square of the surface leads to the decline in the height of the vertices of the surface, which in turn, results in the reduction of contact stress. It causes the surface of the lower height of vertices to remain in elastic regime, compared to that of the higher height of the vertices.

References

[1] Greenwood, J.A., Williamson, J.B., 1966. Contact of nominally flat surfaces. Proceedings: Mathematical, Physical and Engineering Sciences. 295 (1442), 300-319.
[2] Chang, W., Etsion, I., Bogy, D.B., 1987. An elastic-plastic model for the contact of rough surfaces. ASME Journal of Tribology. 109(2), 257-263.
[3] Zhao, Y., Maietta, D.M., Chang, L., 2000. An asperity microcontact model incorporating the transition from elastic deformation to fully plastic flow. ASME Journal of Tribology. 122, 86-93.
[4] Kogut, L., Etsion, I., 2002. Elastic-plastic contact analysis of a sphere and a rigid flat. ASME Journal of Applied Mechanics, 69, 657-662.
[5] Jackson, R., Chusoipin, I., Green, I., 2005. A finite element study of the residual stress and deformation in hemispherical contacts. ASME Journal of Tribology. 127, 484-493.
[6] Jamari, J., Schipper, D.J., 2006. Experimental investigation of fully plastic contact of a sphere against a hard flat. ASME Journal of Tribology. 128, 230-235.
[7] Poon, C.Y., Sayles, R.S., 1994. Numerical contact model of a smooth ball on an anisotropic rough surface. ASME Journal of Tribology. 116, 194-202.
[8] Lee, S.C., Cheng, H.S., 1992. On the relation of load to average gap in the contact between surfaces with longitudinal roughness. Tribology Transactions. 35, 523-529.
[9] Kucharski, S., Klimczak, T., Polijaniuk, A., Kaczmarek, J., 1994. Finite-elements model for the contact of rough surfaces. Wear. 177, 1-13.
[10] Sellgren, U., Björklund, S., Andersson, S., 2003. A finite element-based model of normal contact between rough surfaces. Wear. 2541180-1188.
[11] Pei, L., Hyun, S., Molinari, J., Robbins, M.O., 2005. Finite element modelling of elasto-plastic contact between rough surfaces. Journal of the Mechanics and Physics of Solids. 53, 2385-2409.

[12] Nadimi, S., Otsubo, M., Fonseca, J., Sullivan, C.O., 2019. Numerical modelling of rough particle contacts subject to normal and tangential loading, Granular Matter, 21,108.
[13] Krithivasan, V., Jackson, R.L. 2017. An analysis of three-dimensional elasto-plastic sinusoidal contact. Tribology Letters. 27, 31-43.
[14] Wang, X., Xu, Y., Jackson, R.L., 2017. Elastic–Plastic sinusoidal waviness contact under combined normal and tangential loading. Tribology Letters. 65, 45.
[15] Zhao, B., Zhang, S., Wang, P., Hai, Y., 2015. Loading-unloading normal stiffness model for power-law hardening surfaces considering actual surface topography. Tribology International. 90, 332-342.
[16] Tiwari, A., Wang, A., Müser, M.H., Persson, B.N.J., 2019. Contact mechanics for solids with randomly rough surfaces and plasticity. Lubricants. 7, 90.
[17] Hinkle, A.R., Nöhring, W.G., Leute, R., Junge, T., Pastewka, L., The emergence of small-scale self-affine surface roughness from deformation. Science Advances. 6, 7, 0847.
[18] Venugopalan, S.P., Müser, M.H., Nicola, L., 2017. Green's function molecular dynamics meets discrete dislocation plasticity. Modelling and Simulation in Materials Science and Engineering. 25(6), 065018.
[19] Venugopalan, S.P., Irani, N., Nicola, L., 2019. Plastic contact of self-affine surfaces: Persson's theory versus discrete dislocation plasticity. Journal of the Mechanics and Physics of Solids. 132, 103676.
[20] Irani, N., Nicola, L., 2019. Modelling surface roughening during plastic deformation of metal crystals under contact shear loading. Mechanics of Materials. 132, 66-76.
[21] Venugopalan, S.P., Nicola, L., 2019. Indentation of a plastically deforming metal crystal with a self-affine rigid surface: a dislocation dynamics study. Acta Materialia. 165, 709-721.
[22] Zhang, S., Zhang, Q., 2020. Effects of feed per tooth and radial depth of cut on amplitude parameters and power spectral density of a machined surface. Materials. 13(6), 1323.
[23] Chung, J.C., 2010. Elastic–plastic contact analysis of an ellipsoid and a rigid flat. Tribology International. 43, 491-502.
[24] Ciulli, E., Ferreira, L., Pugliese, G., Tavares, S., 2008. Rough contacts between actual engineering surfaces: Part I. Simple Models for Roughness Description. Wear. 264, 1105-1115.
[25] Patir, N., 1978. A numerical procedure for random generation of rough surfaces. Wear. 47, 263-277.
[26] Newland, D.E., 1984. An introduction to random vibration and spectral analysis 2nd ed., Longman Inc, New York.
[27] Wu, J.J., 2000. Simulation of rough surfaces with FFT. Tribology International. 33, 47-58.
[28] Reizer, R., 2011. Simulation of 3D Gaussian surface topography. Wear. 271, 539-543.
[29] Yastrebov, V.A., Anciaux, G., Molinari, J. F., 2017. On the accurate computation of the true contact-area in mechanical contact of random rough surfaces. Tribology International. 114, 161–171.
[30] Wang, X., Xu, Y., Jackson, R.L., 2018. Theoretical and finite element analysis of static friction between multi-scale rough surfaces. Tribology Letter. 66, 146.
[31] Jacobs, T. D., Junge, T., Pastewka, L., 2018. Quantitative characterization of surface topography using spectral analysis. Surface Topography. 5, No.1, 013001.
[32] Hu, Y., Tonder, K., 1992. Simulation of 3-D random rough surface by 2-D digital filter and Fourier analysis. International Journal of Machine Tools and Manufacture. 32, 83-90.
[33] Onions, R.A., Archard, J.A., 1973. The contact of surfaces having a random structure. Journal of Physics D. 6, 289
[34] Beusink, M., 2011. Measurements and simulations on the (dynamic) properties of aluminium alloy AA6060. Ms.c. Thesis. Department of Mechanical Engineering, Eindhoven University of Technology. Norway